ACS APPLIED MATERIALS & INTERFACES

Letter

www.acsami.org

Functions of Self-Assembled Ultrafine TiO_2 Nanocrystals for High Efficient Dye-Sensitized Solar Cells

Fengxian Xie,[†] Sheng-Jye Cherng,[‡] Shunmian Lu,[†] Ya-Huei Chang,[§] Wei E. I. Sha,[†] Shien-Ping Feng,[§] Chih-Ming Chen,*[,‡] and Wallace C. H. Choy*[,†]

[†]Department of Electrical and Electronic Engineering and [§]Department of Mechanical Engineering, The University of Hong Kong, Pokfulam Road, Hong Kong, China

[‡]Department of Chemical Engineering, National Chung Hsing University, 250, Kuo Kuang Road, Taichung 402, Taiwan

Supporting Information

ABSTRACT: In this paper, we demonstrate a simple approach of self-assembled process to form a very smooth and compacted TiO_2 underlayer film from ultrafine titanium oxide (TiO_2) nanocrystals with dimension of 4 nm for improving the electrical properties and device performances of dye-sensitized solar cells (DSSCs). Because the TiO_2 film self-assembles by simply casting the TiO_2 on fluorine-doped tin oxide (FTO) substrate, it can save a lot of materials in the process. As compared with control DSSC without the self-assembled TiO_2 (SA-TiO_2) layer, short-circuit current density (J_{sc}) improves from 14.9 mA/cm^2 for control DSSC to 17.3 mA/cm^2 for masked DSSC with the SA-TiO_2 layer. With the very smooth SA-TiO_2 layer, the power conversion efficiency is enhanced from 8.22% (control) to 9.35% for the DSSCs with mask and from 9.79% (control) to 11.87% for the DSSCs without mask. To explain the improvement, we have studied the optical properties, morphology, and workfunction of the SA-TiO_2 layer on FTO substrate as well as the impedance spectrum of DSSCs. Importantly, we find that the SA-TiO_2 layers have better morphology, uniformity, and contact with FTO electrode, increased workfunction and optical transmission, as well as reduced charge recombination at the contact of FTO substrate contributing to the improved device performances. Consequently, our results show that the simple self-assembly of TiO_2 ultrafine nanocrystals forms a very good electron extraction layer with both improved optical and electrical properties for enhancing performances of DSSCs.

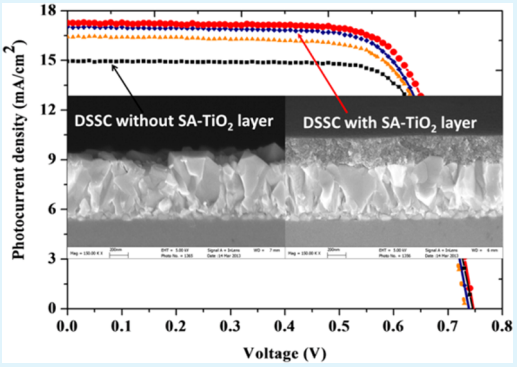

KEYWORDS: *dye-sensitized solar cells (DSSC), ultrafine TiO_2 nanocrystals, self-assemble TiO_2 (SA-TiO_2), morphology, optical properties, workfunction*

INTRODUCTION

Since the demonstration of the first dye-sensitized solar cells (DSSCs) with the interesting features of low cost and high efficiency,[1] various approaches have been investigated to improve the performances of DSSCs such as the introduction of different dye molecule structures, various titanium oxide (TiO_2) nanostructure design, new electrolytes, and nanostructured electrodes. For dye molecule structures, Zn-based porphyrin dye in conjunction with cobalt polypyridyl−based redox electrolytes,[2] alkoxy-wrapped push−pull porphyrins,[3] and zinc phthalocyanines with phosphinic acid anchoring groups[4] have been reported. Regarding the TiO_2 nanostructure layer, nano-embossed hollow spherical TiO_2 (NeHS TiO_2) has been proved to simultaneously offer efficient generation of photo-excited electrons and good light-scattering property.[5] Meanwhile, ZnO-TiO_2 coaxial photoanodes have been introduced to improve the electron transport properties.[6] It is also reported that mesoporous TiO_2 beads with high surface area can enhance the light reflection and external quantum efficiency.[7] Hierarchically structured photoelectrodes are also capable of improving the cell performance due to their special nanostructures based on spherical or one-dimensional assemblies of TiO_2 or ZnO nanocrystallites[8−11] Nanorod-nanosheet hierarchically structured ZnO photoanode has been proved to significantly enhance the photocurrent density of DSSC by increasing the specific surface area.[12] Some works have studied alternative redox mediators as electrolytes such as a eutectic mixture of glycerol and choline iodide of quaternary ammonium salt-derivative ionic liquid,[13] monoelectronic metal-lorganic redox couples of ferrocene/ferrocenium,[14] Ni(III)/Ni(IV) complexes,[15] and Co(II)/Co(III) redox mediators,[16] which show simpler kinetics and may require a smaller energy expenditure for the dye regeneration process, and reduce the associated loss of open-circuit voltage. Meanwhile, solid-state[1721] and quasi-solid-state[22,23] electrolytes have also been

Received: January 30, 2014
Accepted: March 25, 2014
Published: March 26, 2014

   dx.doi.org/10.1021/am5006628 | ACS Appl. Mater. Interfaces 2014, 6, 5367−5373

intensely studied to address the evaporation and leakage issues of liquid electrolyte.

Recently, nanostructured underlayers have been investigated to enhance the electron collection efficiency.[6,24,25] The underlayers have large scale of porous nanostructures with the porous size of few hundred nanometers. By increasing porosity of the layer, the surface area (i.e., aspect ratio) increases and therefore the short-circuit current (J_{sc}), fill factor (FF) and the power conversion efficiency (PCE). Meanwhile, compact TiO_2 by using the approach of soaking the electrode in aqueous $TiCl_4$ solution[26] can also be used to improve electron collection properties and PCE. The hydrolysis of $TiCl_4$ is used to form a compact TiO_2 layer on FTO substrate or ZnO photoanode[27] which can improve carrier transport properties and thus PCE of DSSCs.

In this paper, we demonstrate a new room-temperature approach to form a very smooth and compact TiO_2 underlayer film for enhancing both the optical transmission and electron extraction properties through FTO substrate, and thus device performances of DSSCs improve. Interestingly, the approach of self-assembly TiO_2 (SA-TiO_2) layer by casting ultrafine TiO_2 nanocrystals with an average diameter of about 4 nm on FTO substrate significantly save the materials and has interesting features of better contact with FTO electrode, increased optical transmission and workfunction, prolonged electron lifetime and reduced charge recombination contributing to the improved device performances. As compared with control DSSC without the SA-TiO_2 layer, J_{sc} improves from 14.9 mA/cm^2 (control DSSC) to 17.3 mA/cm^2 for DSSC with the SA-TiO_2 layer. PCE increases from 8.22% (control) to 9.35% (i.e., about 14% enhancement) for the device measured under a light irradiation with mask for confining the exposure area. For sample without mask, PCE well increases from 9.79% (control) to 11.87%. We will also explain the enhancement of DSSC performances by studying the optical properties, morphology, and ultraviolet photoelectron spectroscopy (UPS) of the SA-TiO_2 layer as well as impedance spectrum of DSSCs. As a consequence, our results show that the SA-TiO_2 layer easily formed from TiO_2 ultrafine nanocrystals can be used for enhancing both the electrical and optical performances of DSSCs.

EXPERIMENTAL SECTION

A. Formation of Self-Assembled TiO_2 Films. The ligand-free TiO_2 nanocrystals were synthesized by a nonaqueous method.[28] For our room-temperature self-assembly method, TiO_2 solution was cast onto the desired substrate without spin-coating. The substrate was then quickly covered by a small petri dish. The solution on the substrate then spread to cover the substrate. The vaporization rate of the solvent was controlled within the petri dish. As observed in the experiment, the self-assembly process initially started at the center of the substrate and extended outward while the surrounding TiO_2 nanocrystals gradually packed together to form the film. By varying the nanocrystal concentration and casting volume, we could control the thickness of the film.

Notably, the self-assembly process is sensitive to the selection of solvent. We chose ethanol as the solvent, which is non-toxic and re-disperses the ligand free TiO_2 nanocrystals. The weak intermolecular interactions—hydrogen bond in ethanol—favor the smooth and well-pack film formation. Moreover, the surface tension and viscosity of ethanol is low, indicating that the solution can form good contact with FTO and spread uniformly on the FTO substrate. The vapor pressure of ethanol is low (5.95 kPs at 20 °C), and the ethanol usually evaporates quickly. In our experiment, the FTO substrate was covered quickly after the solution dropped on the substrate. The growth time of the film could then be extended longer to allow TiO_2 nanocrystals with sufficient time to self-organize into well-packed and smooth film.

B. Preparation of DSSC. Fluorine-doped tin oxide glass (FTO glass, 3.1 mm thick, 10 Ω/sq, Tripod Tech) was cleaned in detergent (4% of PK-LCG545) in an ultrasonic bath for 30 min, followed by rinsing with deionized water. Proper amounts of nanocrystalline TiO_2 paste (Ti-Nanoxide T20/SP, Solaronix) was screen-printed (200 mesh) on the FTO glass with and without the new SA-TiO_2 layer using a semi-automatic screen printer (ATMA, AT-45PA). After sintering sequentially in an oven at 325 °C for 5 min, 375 °C for 5 min, 450 °C for 15 min, and 500 °C for 15 min,[29] a 12 μm thick TiO_2 mesoporous film of 0.16 cm^2 area was formed on the FTO glass. The TiO_2 electrode was then immersed in a 0.4 mM N719 dye solution (Everlight Chemical) with ethanol (>99.5%, J.T. Baker). The dye impregnation was conducted at room temperature for 4 h to allow dye adsorption on the TiO_2 nanoparticles.

The tin-doped indium oxide glass (ITO glass sheet, 1.1 mm thick, 7 Ω/sq, Gem Tech) with pre-drilled injection holes was used as the counter electrode. The ITO substrate was firstly rinsed in an aqueous bath containing 4% commercial TCO cleaner and then was immersed into a solution containing 4% conditioner (ML371, Rockwood) at 70°C for 5 min. This treatment changed the surface charge state of the ITO surface to facilitate nanoparticles adsorption. The conditioned substrate was then immersed into nano-Pt ink to adsorb Pt nanoparticles as the counter electrode.[30,31]

The dye-adsorbed TiO_2 photoanode and the Pt-coated counter electrode were laminated face-to-face and sealed with a 25-μm-thick thermal-plastic Surlyn spacer (SX1170-25, Solaronix). A liquid electrolyte, which contained 0.2 M PMII (1-methyl-3-propylimidazolium iodide), 0.05 M I_2, 0.1 M LiI (lithium iodide), 0.2 M TBAI (tetrabutylammonium iodide), 0.5 M TBP (4-tert-butylpyridine) in AN/VN (acetonitrile/valeronitrile) with a specific volume ration (85:15), was injected into the gap between two electrodes via a predrilled hole on the counter electrode side. Finally, the injection holes were hot sealed with a transparent tape.

C. Measurements and Characterizations. UPS measurement was taken by He I discharge lamp (Kratos Analytical) with energy of 21.22 eV and a resolution of 0.15 eV. A −10 V bias was added on samples to enhance the measured signals. The field-emission transmission electron microscope (TEM) image of TiO_2 nanocrystal was measured using Philips Tecnai G2 20 S-TWIN. The cross-section morphology of samples was characterized using field-emission scanning electron microscopy (SEM) (Hitachi S-4800). AFM morphology characterization was performed by using a Digital Instruments NanoScope III in the tapping mode. Transmittance measurement was conducted by spectroscopic ellipsometry (Woollam) under dark.

The fabricated DSSC was evaluated under AM1.5 front-side illumination with a solar simulator (YSS-E40, Yamashita Denso Corp., Japan). A black tape mask with an aperture area of 0.25 cm^2 was covered on the illuminated side of DSSC to reduce the edge effect. Photocurrent−voltage (J−V) curves were recorded using a computer controlled digital source meter (model 2400, Keithley Instruments Inc., USA). The electrochemical impedance spectra of DSSC were also recorded using a potentiostat/galvanostat (PGSTAT 302N, Autolab, Eco-Chemie, Netherlands) under 100 mW cm^{-2} light intensity in the frequency range of 1×10^{-1} to 1×10^5 Hz. The impedance spectra were measured by applying a DC bias at open-circuit voltage and an AC voltage with amplitude of 10 mV. The electron transport property in DSSC was measured using intensity modulated photocurrent spectroscopy (IMPS) and intensity modulated photovoltage spectroscopy (IMVS) with a PGSTAT 302N. A light-emitting diode (LED, 625 nm) with a light intensity up to 6.36 M_w/cm^{-2} was used as the light source. The frequency range is 10 kHz to 1 Hz.

RESULTS AND DISCUSSION

The SA-TiO_2 film is formed at room temperature by casting TiO_2 nanoparticles. The details of forming the TiO_2 nanoparticles and films are described in the Experimental Section. As

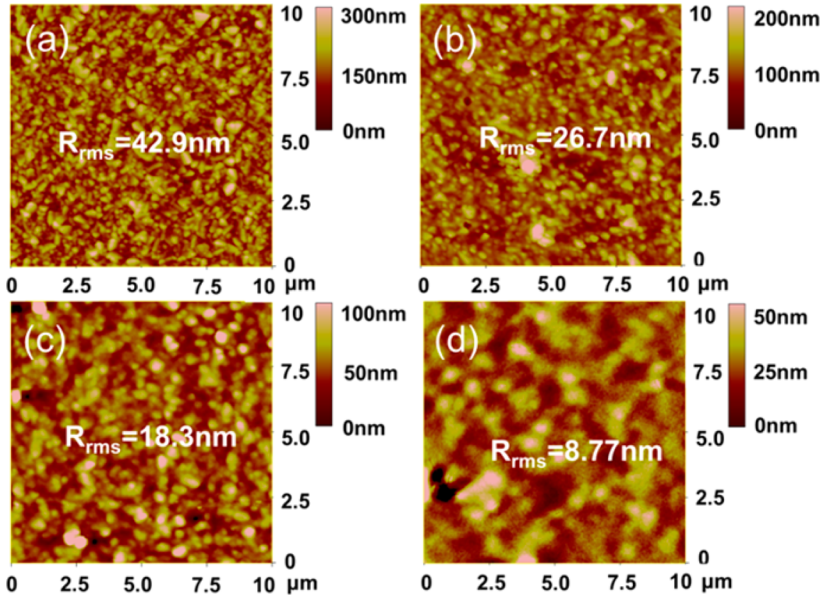

Figure 1. AFM image of samples (a) FTO, (b) SA-TiO_2 100 nm on FTO, (c) SA-TiO_2 300 nm on FTO, (d) SA-TiO_2 590 nm on FTO. Note: the scale of scale bar reduces step-by-step from 300 nm in a to 50 nm in d, i.e. the film becomes smoother when SA-TiO_2 thickness increases.

shown in Figure S1 in the Supporting Information, the results of powder X-ray Diffraction (XRD) ray and field-emission transmission electron microscopy (FE-TEM) show that TiO_2 nanoparticles are nanocrystals with diameter of about 4 nm. The crystal planes of the nanocrystals are identified and shown in Figure S1 in the Supporting Information. In the formation of SA-TiO_2 films, we find that in an ambient and open environment, the TiO_2 nanocrystals in ethanol quickly vaporize, which may cause an unexpected inhomogeneous film. Here, after casting the TiO_2 nanocrystal solvent on FTO substrate without the assistance of any equipment, we quickly cover the sample by a small petri dish to control the vaporization rate of ethanol at room temperature. From our observation, the self-assembly process initially starts at the center of the FTO substrate. Interestingly, the surrounding nanocrystals then gradually pack into smooth film when the solvent slowly vaporizes. The thickness of SA-TiO_2 films can be easily controlled by varying TiO_2 nanocrystal concentration and casting volume of TiO_2 solution. (The thicknesses of TiO_2 films are determined from the cross-section scanning electron microscope (SEM) measurement.)

The images of atomic force microscopy (AFM) of FTO substrate with different thicknesses of SA-TiO_2 films are shown in Figure 1. (The AFM phase images are shown in Figure S2 in the Supporting Information). It can be observed that the roughness reduces through increasing the thickness of SA-TiO_2 films on FTO from rms roughness (R_{rms}) of 42.9 nm (bare FTO) to R_{rms} of 26.7 nm (100 nm SA-TiO_2 film on FTO), R_{rms} of 18.3 nm (300 nm SA-TiO_2 film), and R_{rms} of 8.77 nm (590 nm SA-TiO_2 film). It should be noted that the scale of the scale bar reduces step-by-step from 300 nm in Figure 1a to 10 nm in Figure 1d, i.e., the film becomes smoother when SA-TiO_2 thickness increases. Importantly, the AFM phase images in Figure S2 in the Supporting Information indicate that when the SA-TiO_2 thickness increases, the TiO_2 will have better coverage on FTO, which will favor the electron collection of FTO electrode and improve device performance as will be discussed below.

To intuitively demonstrate the contribution of the SA-TiO_2, DSSCs with the commonly used dye of N719 but different thicknesses of the SA-TiO_2 films have been fabricated. Details of device fabrication have been described in the Experimental Section. The current density (J)−voltage (V) characteristics of DSSCs measured with light irradiated mask are shown in Figure 2 and the performance parameters including open-circuit

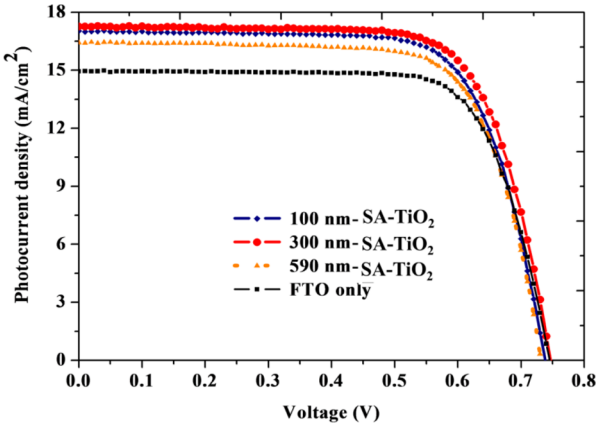

Figure 2. J−V curve (measured with mask for confining the exposure area) of DSSCs with different thickness of the SA-TiO_2 layer.

voltage (V_{oc}), J_{sc}, fill factor (FF), and PCE are listed in Table 1. It can be observed that when thickness of the SA-TiO_2 film is

Table 1. Performances (measured with mask for confining the irradiation area) of DSSC with Different Thicknesses Of SA-TiO_2

OSCs	J_{sc} (mA/cm^2)	V_{oc} (V)	fill factor	PCE (%)
FTO	14.937	0.746	0.737	8.217
100 nm SA-TiO_2	17.030	0.738	0.717	9.022
300 nm SA-TiO_2	17.258	0.747	0.725	9.349
590 nm SA-TiO_2	16.424	0.732	0.725	8.716

dx.doi.org/10.1021/am5006628 | ACS Appl. Mater. Interfaces 2014, 6, 5367−5373

increased from 0 nm (control device) to 100 nm, J_{sc} increases to 17.03 as compared to 14.937 mA/cm^2 (control). The J_{sc} then peaks with a value of 17.258 mA/cm^2 when the thickness is increased to 300 nm. When the thickness is further increased to 590 nm, J_{sc} reduces to 16.424 mA/cm^2 (still better than that of control DSSC). Meanwhile, V_{oc} and *FF* do not change obviously. As a result, PCE increases from 8.21 to 9.35% (the optimized case with 300 nm of SA-TiO_2 film) with enhancement of about 14%. It should be noted that J_{sc} (PCE) of DSSCs without mask further increase from 17.84 mA/cm^2 (9.79%) to 21.99 mA/cm^2 (11.87%) for the optimized case with 300 nm of SA-TiO_2 film due to the light collection from the edge of the device (device results are shown in Table S1 in the Supporting Information). As a consequence, the introduction of the SA-TiO_2 film on FTO substrate can significantly increase J_{sc} and thus PCE. To understand the improvement, we will investigate the physical, optical, and electrical properties of the SA-TiO_2 films in DSSCs.

The cross-sections of the films have been investigated by using field-emission scanning electron microscope (SEM) as shown in Figure 3. It can be observed that the SA-TiO_2 film (Figure 3b) formed from the ultrafine TiO_2 nanocrystals has better film quality as compared to the film formed from the conventional anatase TiO_2 nanoparticles used in DSSC (about 30 nm size) (Figure 3c). In addition, the SA-TiO_2 films have better (tight) contact to the FTO substrate while there is a clear space/voids between the conventional anatase TiO_2 nanoparticles and FTO substrate as shown in Figure 3c. The interesting features of the casted SA-TiO_2 films contribute to better electrical properties of DSSCs as described later.

Besides the film quality, we also investigate the optical properties of the SA-TiO_2 films. From the transmission spectra as shown in Figure 4, it is interesting to note that oscillations form when TiO_2 films are self-assembled/casted on the FTO substrate. Since the SA-TiO_2 films are very smooth (see Figure 3b) as compared to FTO surface, Fabry-Perot modes form at some specific and well separated wavelengths. Therefore, the transmission spectra become oscillatory. However, the transmission spectrum of bare FTO is smooth because FTO surface is very rough as shown in Figure 4. At this time, rough FTO can be regarded as a superposition of smooth FTOs with different thicknesses. Hence, the total internal reflection can be easily supported at more wavelengths and guided mode resonance will be broadened in the rough FTO structure. As a result, the transmission spectrum becomes smooth. Consequently, the oscillating behavior of the transmission spectra of the SA-TiO_2 coated FTO re-confirm that the TiO_2 film is physically smoother than the bare FTO film.

Regarding the transmission value, transmission of FTO with different thicknesses of SA-TiO_2 film is generally similar because the absorption of TiO_2 is very low. The light absorption loss in SA-TiO_2 at different thicknesses is similar and ignorable, which is also confirmed from the diffused absorption spectra. Even though the thickness of SA-TiO_2 changes from 100 nm to 590 nm, there is no clear change in the transmittance as shown in Figure 4. However, when SA-TiO_2 thickness increases, the oscillation of transmission spectrum increases (becomes more condense) as shown in Figure 4. Importantly, the transmission of SA-TiO_2 films is generally better than bare FTO due to the fact that the rough surface of bare FTO enhances light trapping in the structure by multiple total internal reflections resulting in reduced light penetration. According to statistical ray optics theory by Yablonovitch,[32]

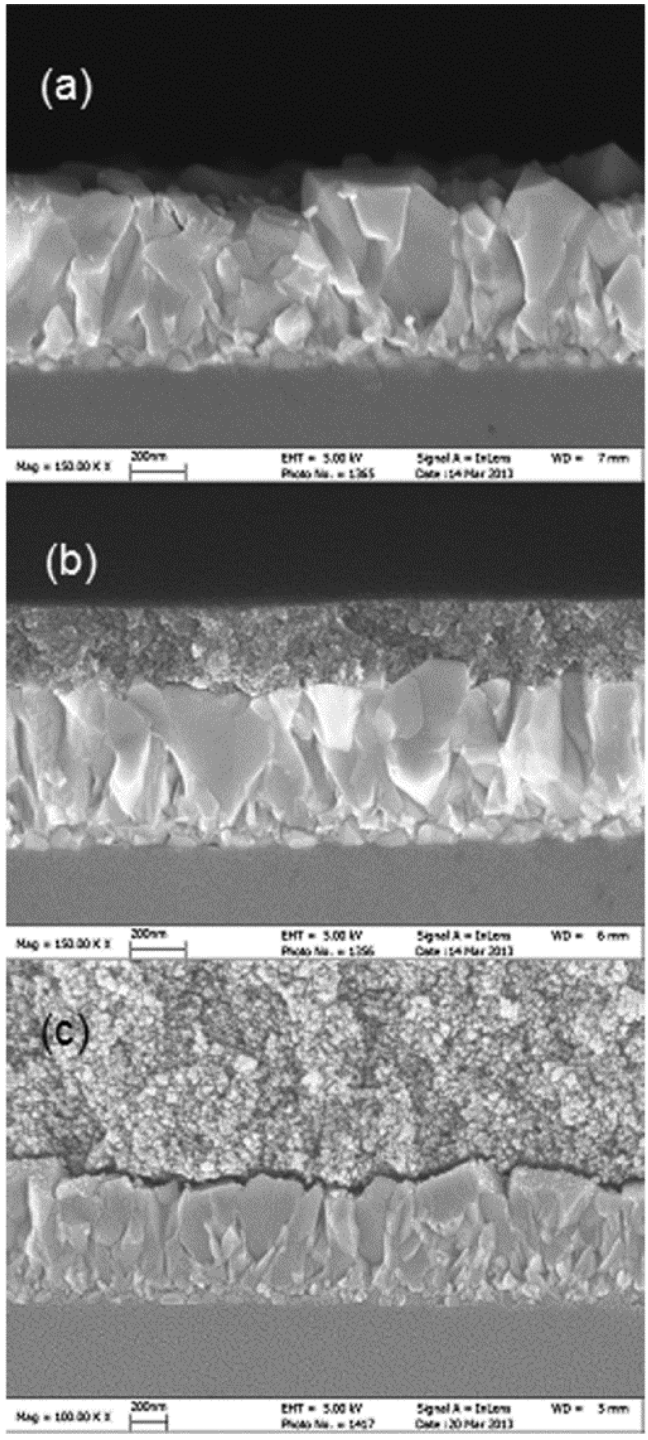

Figure 3. Cross-section SEM pictures of samples. (a) Bare FTO on glass, (b) 300 nm thick SA-TiO_2 film on FTO, and (c) TiO_2 (with diameter of about 30 nm) mesoporous film on FTO substrate.

strongly textured rear or front surface can result in an isotropic distribution of photons inside; and light absorption enhancement can be obtained. The transmission of FTO/SA-TiO_2 improves more at short wavelengths as compared to bare FTO. It is because when wavelength reduces, the excited guided modes (i.e., trapped light) of bared FTO increases. By forming the smooth SA-TiO_2 film on the FTO, the transmission can be improved more at short wavelengths. To summarize, with the insertion of smooth SA-TiO_2 film, the transmission of the

dx.doi.org/10.1021/am5006628 | ACS Appl. Mater. Interfaces 2014, 6, 5367−5373

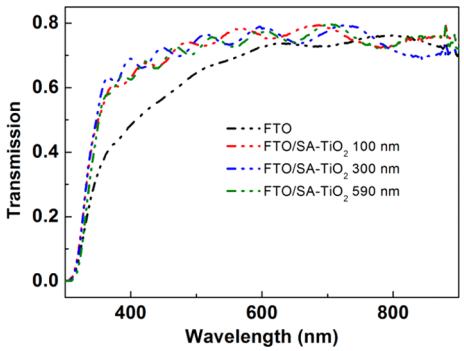

Figure 4. Diffused transmission spectra of treated FTO glasses with different thickness of SA-TiO_2 layer.

sample generally improve (particularly in the short wavelength region) and optically favors the use as transparent electrode for DSSCs.

Meanwhile, we make an estimation of the increased Jsc from transmission spectrum by assuming the internal quantum efficiency (IQE) is 100%. The J_{sc} improvement due to the increased transmission is 1.5 mA/cm^2. From our experimental results, J_{sc} is totally increased by 2.4 mA/cm^2. This implies that the improvement of the device performance is not just contributed from the optical effects, and at least 0.9 mA/cm^2 is contributed from electrical improvement due to the introduction of the SA-TiO_2 film as discussed below.

To understand the electrical properties of the SA-TiO_2 film on FTO, we have investigated the bandstructures of various FTO/SA-TiO_2 samples by measuring ultraviolet photoelectron spectroscopy (UPS) as shown in Figure 5. In order to

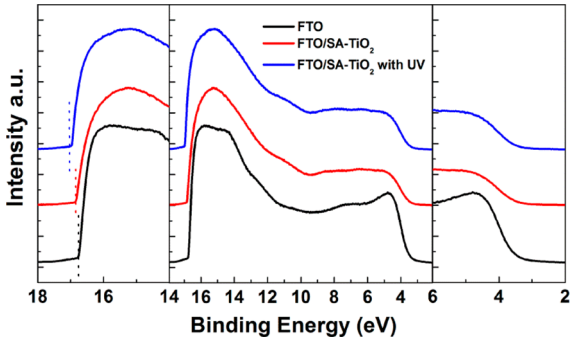

Figure 5. UPS spectra of FTO/SA-TiO_2 layer with and without UV illumination: photoemission onset (left); full valence spectra (middle); density of states near the oxide valence band edge (right).

determine the workfunction of the samples, we extract the Fermi edge and secondary-electron cut-off from the UPS spectrum as shown in Table 2. Since the workfunction of FTO is 4.9 eV,[33] the workfunction of FTO/SA-TiO_2 (300 nm) before and after the exposure of UV from sun-simulator can be determined as 4.74 and 4.51 eV, respectively. This means that by forming the SA-TiO_2 on FTO, the Fermi level shifted upward by 0.16 eV, which favors the electron extraction of DSSC to the electrode. In addition, with exposure of the UV from sunlight (generated by sun-simulator), the Fermi level can further shift up by 0.39 eV because of the accumulation of photogenerated carriers in the SA-TiO_2 layer. As a result, the introduction of SA-TiO_2 layer can enhance the electron extraction by reducing the potential barrier and thus the electrical properties of DSSCs.

Table 2. The bandstructure parameter of FTO with and without SA-TiO_2 layer

	FTO (eV)	FTO/SA-TiO_2 (300 nm) (eV)	FTO/SA-TiO_2 (300 nm) UV (eV)
Fermi edge	3.52	3.45	3.39
secondary-electron cut-off	16.76	16.85	17.02
work function	4.90	4.74	4.51
E_F shift compared to FTO		−0.16	−0.39

The improvement of interfacial properties by introducing the SA-TiO_2 layer can also be explained from the impedance measurement. The Nyquist plot and Bode plot are shown in Figure 6 and Figure S3 in the Supporting Information. From the Nyquist plot, it is observed that the impedance at low frequency region is very similar for DSSCs with and without the SA-TiO_2 layers. It is reasonable because the frequency region corresponds to the TiO_2 active layer and electrolyte rather than our SA-TiO_2 layer. For the control DSSC without the SA-TiO_2 layer, the impedance at high frequency (Figure 6a) is derivated from ideal semi-spherical shape due to the super-imposed impedance corresponding to Pt electrode and the contact of conventional anatase TiO_2 NPs to FTO electrode. The impedance at high frequency at the conventional anatase TiO_2 NP/FTO contact indicates that some carriers will quickly recombine at around the FTO contact which will degrade device performance. Interestingly, with the insertion of the SA-TiO_2 layer (Figure 6a−d), the high-frequency impedance splits into two parts obviously. From Bode plot (see Figure S2e−h in the Supporting Information), we find that there is a merged frequency peak corresponding to the Pt electrode and the anatase TiO_2 NP/FTO contact. By introducing our SA-TiO_2 layer on FTO, the corresponding frequency of the TiO_2 NP/FTO contact present high frequency as shown in Figure S3f−h in the Supporting Information. This implies that the carrier recombination at the ITO contact is diminished and thus performances of DSSCs improve.

On the basis of the above results, the SA-TiO_2 layer of 300 nm shows the best performance. When the SA-TiO_2 layer increases from 100 nm to 300 nm, the efficiency is improved because the compact SA-TiO_2 layer can effectively reduce the recombination (as from the analysis of Bode plots in Figure S3 in the Supporting Information). Moreover, from the AFM phase results as shown in Figure S2 in the Supporting Information, we can find that the coverage of the compact SA-TiO_2 layer on FTO improves which will favor the electron collection of the FTO electrode. For instance, as shown in Figure S2b in the Supporting Information, the uniformity of 100 nm SA-TiO_2 on top of FTO is relatively poorer compared to 300 nm and 590 nm in Figure S2c, d in the Supporting Information, which will reduce the contact between the mesoporous TiO_2 and FTO and thus reduces the electron collection. Furthermore, it is interesting to note that the transmission of FTO with SA-TiO_2 almost keeps unchanged when thickness increasing from 100 nm to 590 nm and is all better than that of the bare FTO substrate as mentioned previously. It is the SA-TiO_2 layer induced series resistance that accounts for the decreased performance from 300 nm to 590 nm as shown in Table S2 in the Supporting Information. Consequently, the competition of the above effects with

dx.doi.org/10.1021/am5006628 | ACS Appl. Mater. Interfaces 2014, 6, 5367−5373

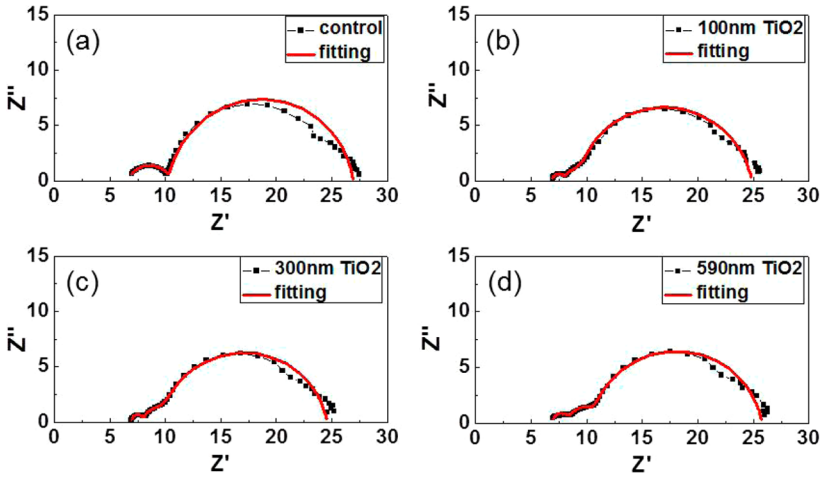

Figure 6. Nyquist plot of DSSCs with different thicknesses of SA-TiO_2 film.

increased TiO_2 thickness results in the best 300 nm SA-TiO_2 layer performance.

CONCLUSION

In this work, we have proposed and demonstrated the introduction of a SA-TiO_2 film on FTO to improve performances of DSSCs. The formation of the film is material saving and can be easily fabricated by simply casting the TiO_2 nanocrystal solution on FTO substrate. The process of forming TiO_2 nanocrystal solution is performed under room temperature, which is simpler compared to a few degree calices required by TiO_2 formed from hydrolysis of $TiCl_4$. Importantly, our results show that the SA-TiO_2 layer have better morphology, uniformity, and contact with FTO electrode, increased workfunction and optical transmission, as well as reduced charge recombination contributing to the improved device performances. As compared with control DSSC without the SA-TiO_2 layer, short-circuit current improves from 14.9 mA/cm^2 for control DSSC to 17.3 mA/cm^2 for masked DSSC with the SA-TiO_2 layer. The power conversion efficiency enhances by about 14 from 8.22% (control) to 9.35% for the DSSCs with the SA-TiO_2 layer. Consequently, our results show that the simple self-assembly of TiO_2 ultrafine nanocrystals forms a very good electron extraction layer for enhancing performances of DSSCs.

ASSOCIATED CONTENT

Supporting Information

Additional information details about X-ray diffraction (XRD) and field-emission transmission electron microscopy (FE-TEM) images of ultrafine TiO_2 nanocrystals, AFM phase images of different thickness of SA-TiO_2 on FTO, impedance model and parameter, DSSC (without mask) performances with and without the optimized SA-TiO_2. This material is available free of charge via the Internet at http://pubs.acs.org.

AUTHOR INFORMATION

Corresponding Authors

*E-mail: chchoy@eee.hku.hk. Fax: (852) 25598738.
*E-mail: chencm@nchu.edu.tw.

Author Contributions

The manuscript was written through contributions of all authors. All authors have given approval to the final version of the manuscript.

Notes

The authors declare no competing financial interest.

ACKNOWLEDGMENTS

This work is supported by University Grant Council of the University of Hong Kong (Grants 10401466 and 201111159062), and the General Research Fund (Grants HKU#712010E and HKU711612E), the RGC-NSFC grant (N_HKU709/12) and the SRFDP and RGC ERG Joint Research Scheme (M-HKU703/12) from the Research Grants Council (RGC) of Hong Kong Special Administrative Region, China.

ABBREVIATIONS

TiO_2, titanium oxide
DSSCs, dye-sensitized solar cells
SA-TiO_2, self-assembled TiO_2
J_{sc}, short-circuit current density
FF, fill factor
PCE, power conversion efficiency
UPS, ultraviolet photoelectron spectroscopy
XRD, X-ray diffraction
FE-TEM, field-emission transmission electron microscopy
AFM, atomic force microscopy
SEM, scanning electron microscope

REFERENCES

(1) O'Regan, B.; Gratzel, M. A Low-Cost, High-Efficiency Solar Cell Based on Dye-Sensitized Colloidal TiO_2 Films. *Nature* **1991**, *353* (6346), 737−740.
(2) Yella, A.; Lee, H.-W.; Tsao, H. N.; Yi, C.; Chandiran, A. K.; Nazeeruddin, M. K.; Diau, E. W.-G.; Yeh, C.-Y.; Zakeeruddin, S. M.; Grätzel, M. Porphyrin-Sensitized Solar Cells with Cobalt (II/III)−based Redox Electrolyte Exceed 12 Percent Efficiency. *Science* **2011**, *334* (6056), 629−634.
(3) Ripolles-Sanchis, T.; Guo, B.-C.; Wu, H.-P.; Pan, T.-Y.; Lee, H.-W.; Raga, S. R.; Fabregat-Santiago, F.; Bisquert, J.; Yeh, C.-Y.; Diau, E. W.-G. Design and Characterization of Alkoxy-Wrapped Push−Pull Porphyrins for Dye-Sensitized Solar Cells. *Chem. Commun.* **2012**, *48* (36), 4368−4370.
(4) López-Duarte, I.; Wang, M.; Humphry-Baker, R.; Ince, M.; Martínez-Díaz, M.; Nazeeruddin, M. K.; Torres, T.; Grätzel, M. Molecular Engineering of Zinc Phthalocyanines with Phosphinic Acid Anchoring Groups. *Angew. Chem.* **2012**, *124* (8), 1931−1934.

(5) Koo, H. J.; Kim, Y. J.; Lee, Y. H.; Lee, W. I.; Kim, K.; Park, N. G. Nano-embossed Hollow Spherical TiO2 as Bifunctional Material for High-Efficiency Dye-Sensitized Solar Cells. *Adv. Mater.* **2008**, *20* (1), 195−199.
(6) Williams, V. O.; Jeong, N. C.; Prasittichai, C.; Farha, O. K.; Pellin, M. J.; Hupp, J. T. Fast Transporting ZnO−TiO_2 Coaxial Photoanodes for Dye-Sensitized Solar Cells Based on ALD-Modified SiO_2 Aerogel Frameworks. *ACS Nano* **2012**, *6* (7), 6185−6196.
(7) Chen, D.; Huang, F.; Cheng, Y.-B.; Caruso, R. A. Mesoporous Anatase TiO_2 Beads with High Surface Areas and Controllable Pore Sizes: A Superior Candidate for High-Performance Dye-Sensitized Solar Cells. *Adv. Mater.* **2009**, *21* (21), 2206−2210.
(8) Dutta, S.; Patra, A. K.; De, S.; Bhaumik, A.; Saha, B. Self-Assembled TiO_2 Nanospheres by Using a Biopolymer as a Template and Its Optoelectronic Application. *ACS Appl. Mater. Interfaces* **2012**, *4* (3), 1560−1564.
(9) Zhang, Q.; Cao, G. Hierarchically Structured Photoelectrodes for Dye-sensitized Solar Cells. *J. Mater. Chem.* **2011**, *21* (19), 6769−6774.
(10) Tian, J.; Zhang, Q.; Uchaker, E.; Liang, Z.; Gao, R.; Qu, X.; Zhang, S.; Cao, G. Constructing ZnO Nanorod Array Photoelectrodes for Highly Efficient Quantum Dot Sensitized Solar Cells. *J. Mater. Chem. A* **2013**, *1* (23), 6770−6775.
(11) De, S.; Dutta, S.; Patra, A. K.; Bhaumik, A.; Saha, B. Self-assembly of Mesoporous TiO_2 Nanospheres Viaaspartic Acid Templating Pathway and its Catalytic Application for 5-hydroxymethyl-furfural Synthesis. *J. Mater. Chem.* **2011**, *21* (43), 17505−17510.
(12) Gao, R.; Liang, Z.; Tian, J.; Zhang, Q.; Wang, L.; Cao, G. ZnO Nanocrystallite Aggregates Synthesized through Interface Precipitation for Dye-Sensitized Solar Cells. *Nano Energy* **2013**, *2* (1), 40−48.
(13) Jhong, H.-R.; Wong, D. S.-H.; Wan, C.-C.; Wang, Y.-Y.; Wei, T.-C. A Novel Deep Eutectic Solvent-Based Ionic Liquid used as Electrolyte for Dye-Sensitized Solar Cells. *Electrochem. Commun.* **2009**, *11* (1), 209−211.
(14) Daeneke, T.; Kwon, T.-H.; Holmes, A. B.; Duffy, N. W.; Bach, U.; Spiccia, L. High-efficiency Dye-sensitized Solar Cells with Ferrocene-based Electrolytes. *Nat. Chem.* **2011**, *3* (3), 211−215.
(15) Li, T. C.; Spokoyny, A. M.; She, C.; Farha, O. K.; Mirkin, C. A.; Marks, T. J.; Hupp, J. T. Ni (III)/(IV) bis (dicarbollide) as a Fast, Noncorrosive Redox Shuttle for Dye-Sensitized Solar Cells. *J. Am. Chem. Soc.* **2010**, *132* (13), 4580−4582.
(16) Mosconi, E.; Yum, J.-H.; Kessler, F.; Gómez García, C. J.; Zuccaccia, C.; Cinti, A.; Nazeeruddin, M. K.; Grätzel, M.; De Angelis, F. Cobalt Electrolyte/Dye Interactions in Dye-Sensitized Solar Cells: A Combined Computational and Experimental Study. *J. Am. Chem. Soc.* **2012**, *134* (47), 19438−19453.
(17) Chung, I.; Lee, B.; He, J.; Chang, R. P. H.; Kanatzidis, M. G. All-Solid-State Dye-Sensitized Solar Cells with High Efficiency. *Nature* **2012**, *485* (7399), 486−489.
(18) Cai, N.; Moon, S.-J.; Cevey-Ha, L.; Moehl, T.; Humphry-Baker, R.; Wang, P.; Zakeeruddin, S. M.; Grätzel, M. An Organic D-π-A Dye for Record Efficiency Solid-State Sensitized Heterojunction Solar Cells. *Nano Lett.* **2011**, *11* (4), 1452−1456.
(19) Li, Q.; Zhao, J.; Sun, B.; Lin, B.; Qiu, L.; Zhang, Y.; Chen, X.; Lu, J.; Yan, F. High-Temperature Solid-State Dye-Sensitized Solar Cells Based on Organic Ionic Plastic Crystal Electrolytes. *Adv. Mater.* **2012**, *24* (7), 945−950.
(20) Wang, H.; Zhang, X.; Gong, F.; Zhou, G.; Wang, Z.-S. Novel Ester-Functionalized Solid-state Electrolyte for Highly Efficient All-Solid-State Dye-sensitized Solar Cells. *Adv. Mater.* **2012**, *24* (1), 121−124.
(21) Akhtar, M. S.; Kwon, S.; Stadler, F. J.; Yang, O. B. High Efficiency Solid State Dye Sensitized Solar Cells with Graphene-Polyethylene Oxide Composite Electrolytes. *Nanoscale* **2013**, *5* (12), 5403−5411.
(22) Yu, Z.; Qin, D.; Zhang, Y.; Sun, H.; Luo, Y.; Meng, Q.; Li, D. Quasi-Solid-State Dye-Sensitized Solar Cell Fabricated with Poly([small beta]-hydroxyethyl methacrylate) Based Organogel Electrolyte. *Energy Environ. Sci.* **2011**, *4* (4), 1298−1305.
(23) Zhao, J.; Shen, X.; Yan, F.; Qiu, L.; Lee, S.; Sun, B. Solvent-Free Ionic Liquid/Poly(ionic liquid) Electrolytes for Quasi-Solid-State Dye-Sensitized Solar Cells. *J. Mater. Chem.* **2011**, *21* (20), 7326−7330.
(24) An, J.; Guo, W.; Ma, T. Enhanced Photoconversion Efficiency of All-Flexible Dye-Sensitized Solar Cells Based on a Ti Substrate with TiO2 Nanoforest Underlayer. *Small* **2012**, *8* (22), 3427−3431.
(25) Wei, T.-C.; Wan, C.-C.; Wang, Y.-Y.; Chen, C.-m.; Shiu, H.-s. Immobilization of Poly(N-vinyl-2-pyrrolidone)-capped Platinum Nanoclusters on Indium−Tin Oxide Glass and Its Application in Dye-Sensitized Solar Cells. *J. Phys. Chem. C* **2007**, *111* (12), 4847−4853.
(26) Burke, A.; Ito, S.; Snaith, H.; Bach, U.; Kwiatkowski, J.; Grätzel, M. The Function of a TiO2 Compact Layer in Dye-Sensitized Solar Cells Incorporating "Planar" Organic Dyes. *Nano Lett.* **2008**, *8* (4), 977−981.
(27) Sakai, N.; Miyasaka, T.; Murakami, T. N. Efficiency Enhancement of ZnO-Based Dye-Sensitized Solar Cells by Low-Temperature $TiCl_4$ Treatment and Dye Optimization. *J. Phys. Chem. C* **2013**, *117* (21), 10949−10956.
(28) Jensen, G. V.; Bremholm, M.; Lock, N.; Deen, G. R.; Jensen, T. R.; Iversen, B. B.; Niederberger, M.; Pedersen, J. S.; Birkedal, H. Anisotropic Crystal Growth Kinetics of Anatase TiO_2 Nanoparticles Synthesized in a Nonaqueous Medium. *Chem. Mater.* **2010**, *22* (22), 6044−6055.
(29) Ito, S.; Ha, N.-L. C.; Rothenberger, G.; Liska, P.; Comte, P.; Zakeeruddin, S. M.; Pechy, P.; Nazeeruddin, M. K.; Gratzel, M. High-Efficiency (7.2%) Flexible Dye-Sensitized Solar Cells with Ti-Metal Substrate for Nanocrystalline-TiO_2 Photoanode. *Chem. Commun.* **2006**, *38*, 4004−4006.
(30) Wei, T.-C.; Wan, C.-C.; Wang, Y.-Y.; Chen, C.-m.; Shiu, H.-s. Immobilization of Poly(N-vinyl-2-pyrrolidone)-Capped Platinum Nanoclusters on Indium-Tin Oxide Glass and Its Application in Dye-Sensitized Solar Cells. *J. Phys. Chem. C* **2007**, *111* (12), 4847−4853.
(31) Wei, T.; Wan, C.; Wang, Y. Poly(N-vinyl-2-pyrrolidone)-Capped Platinum Nanoclusters on Indium-Tin Oxide Glass as Counterelectrode for Dye-Sensitized Solar Cells. *Appl. Phys. Lett.* **2006**, *88* (10), 103122−3.
(32) Yablonovitch, E. Statistical Ray Optics. *J. Opt. Soc. Am.* **1982**, *72* (7), 899−907.
(33) Xiao, W.; Tengfeng, X.; Dan, X.; Qidong, Z.; Shan, P.; Dejun, W. A Study of the Dynamic Properties of Photo-Induced Charge Carriers at Nanoporous TiO_2/Conductive Substrate Interfaces by the Transient Photovoltage Technique. *Nanotechnology* **2008**, *19* (27), 275707.